Progress in PHOTOVOLTAICS

PROGRESS IN PHOTOVOLTAICS: RESEARCH AND APPLICATIONS
Prog. Photovolt: Res. Appl. 2016; **24**:517–532
Published online 9 January 2015 in Wiley Online Library (wileyonlinelibrary.com). DOI: 10.1002/pip.2571

29TH EU PVSEC, AMSTERDAM, THE NETHERLANDS 2014

Fault identification in crystalline silicon PV modules by complementary analysis of the light and dark current–voltage characteristics

Sergiu Viorel Spataru[1]*, Dezso Sera[1], Peter Hacke[2], Tamas Kerekes[1] and Remus Teodorescu[1]

[1] Aalborg University, Energy Technology, Pontoppidanstræde 101, Aalborg 9220, Denmark
[2] National Renewable Energy Laboratory (NREL), 15013 Denver W Pkwy, Golden, CO 80401, United States

ABSTRACT

This article proposes a fault identification method, based on the complementary analysis of the light and dark current–voltage (I–V) characteristics of the photovoltaic (PV) module, to distinguish between four important degradation modes that lead to power loss in PV modules: (i) degradation of the electrical circuit of the PV module (cell interconnect breaks; corrosion of the junction box, module cables, and connectors); (ii) mechanical damage to the solar cells (cell microcracks and fractures); (iii) potential-induced degradation (PID) sustained by the module; and (iv) optical losses affecting the module (soiling, shading, and discoloration). The premise of the proposed method is that different degradation modes affect the light and dark I–V characteristics of the PV module in different ways, leaving distinct *signatures*. This work focuses on identifying and correlating these specific signatures present in the light and dark I–V measurements to specific degradation modes; a number of new dark I–V diagnostic parameters are proposed to quantify these signatures. The experimental results show that these dark I–V diagnostic parameters, complemented by light I–V performance and series-resistance measurements, can accurately detect and identify the four degradation modes discussed. Copyright © 2015 John Wiley & Sons, Ltd.

KEYWORDS

fault identification; degradation; dark I–V characteristic; series resistance; cell cracks; optical losses; potential-induced degradation

***Correspondence**

Sergiu Viorel Spataru, Aalborg University, Energy Technology, Pontoppidanstræde 101, Aalborg 9220, Denmark.
E-mail: ssp@et.aau.dk

Received 30 June 2014; Revised 8 October 2014; Accepted 22 October 2014

1. INTRODUCTION

The number of PV system installations has been increasing rapidly in the last several years, reaching a global cumulative installed capacity of 138.9 GW at the end of 2013 [1]. With the decreasing cost of PV modules [2] and balance-of-systems components [3], the plant operating cost becomes more relevant in reducing the total lifetime cost of the plant. Therefore, PV system monitoring and diagnostic tools are increasingly important in identifying and understanding the failures and degradation modes affecting PV modules. By doing this, we can design more reliable PV modules, take corrective actions in the case of incipient failures before they develop into major defects, or optimize the maintenance of the PV plant.

The diagnostic methods required for identifying the cause of degradation and power loss within a module largely depend on the degradation mode itself, and may require a specialized diagnostic process or on-site personnel, which adds to system operations costs and may not always be feasible. Although in practice PV modules can be affected by a large variety of failures, this article will focus on investigating four important degradation modes that lead to power loss in PV modules, as described in the next paragraphs.

Optical losses can occur due to a series of factors that affect the optical layer of the PV module and reduce the amount of light reaching the cell surface. The most common of these factors are: soiling and shading [4,5], encapsulant discoloration or delamination [6,7], front-glass corrosion or breakage [6], and deterioration of the antireflection coating [4,8]. Factors causing optical losses leave a visual impact on the PV module's surface and can be relatively easily detected through visual inspection [4,6]. Certain types of partial shading can be detected from the distortion they cause in the light I–V characteristic [9,10],

whereas more generic fault-detection techniques identify shading by correlating power loss with a specific time of day [11] or relative position of the sun [12,13].

The *electrical circuit of a PV module* is composed of cell-interconnect ribbons, wiring, junction box, and connectors that can degrade over time, leading to power loss, and potential hazards [6,14,15]. Disconnected cell and string interconnects are often the result of poor soldering, mechanical stress, and thermal cycling [6,14]. These can give rise to an increase in the module's series resistance [14,15], increased heating in the module, and localized hot spots [8,15]. Fielded modules exhibiting such interconnect failures often go undetected especially in residential PV systems because they require thermal imaging and circuit fault detectors to be identified [16]. Moisture ingress can cause corrosion of the module connectors [17] and of the string interconnects in the junction box [6], manifested as an increase in the PV module's series resistance and power loss [17]. Detecting this type of degradation would require visual inspection or thermal imaging of the cables, connectors, and junction box. An alternative method would be to perform accurate series-resistance measurements at module level [18,19], which would reveal an increase in the module's series resistance.

Mechanical damage to solar cells, such as microcracks and fractures, can occur during the manufacturing process [20], module packaging and transport [21], module installation [6], and operation in the field due to mechanical [22] and thermal stresses [23]. Cell microcracks and breaks have no visual impact on the module surface, except for the so-called "snail tracks" that sometimes appear [6], and they can be difficult to detect without the help of diagnostic tools such as thermography [24] or electroluminescence imaging [25,26].

Potential-induced degradation is a failure mode affecting PV systems that has gained considerable attention in the last few years due to the significant negative impact it can have on the performance of the plant [27–29]. PV modules affected by PID usually do not present any visual symptom, so it is difficult to detect the onset of PID until the degradation becomes severe [6,28]. The most common methods for detecting PID are shunt-resistance measurement [30], thermography [28], electroluminescence imaging [27,28], and measurement of module open-circuit voltage (V_{oc}) at both ends of the string during low light conditions [28,31]. Once PID has been detected in the field, measures can be taken to stop and even reverse (at least, in part) its effect on the modules [27,28].

This work focuses on identifying and correlating specific signatures present in the light and dark I–V measurements, to specific degradation modes. A set of diagnostic parameters are calculated from the dark I–V characteristic that can detect general degradation of the PV module's aggregation of electrical components and solar cells, as well as shunting and recombination losses occurring due to cell cracks, broken cells, and PID. These parameters facilitate the ease of machine analysis for modules degrading nonuniformly across the solar cells, and where curve fitting a solar cell model to analyze the degradation mode, would not be feasible. The dark I–V diagnostic parameters, combined with light I–V performance, and series resistance measurements can accurately detect and identify optical losses, degradation of the electrical circuit, mechanical damage to solar cells, and PID.

The method and results presented in the current work were developed under laboratory conditions and will translate well as a laboratory diagnostic tool for PV modules, in the detection of damaged ribbon interconnects, cell microcracks, fractures, or incipient PID, without the need of thermal or electroluminescence imaging.

The method also has potential for field applications such as implementation in I–V tracers for long-term reliability monitoring of PV modules, with the goal of identifying the onset and progression of the different degradation modes, without the need of periodic inspection and imaging. Another possible application would be in module-integrated converters capable of bidirectional current flow, where the method can be used to optimize maintenance operations by scheduling appropriate actions based on the severity and type of degradation affecting the PV modules. Implementing the method for outdoor operation needs to take into consideration the changing ambient conditions, as well as other practical implementation issues; however, this falls outside the scope of the current work and is anticipated to be developed in the future.

This paper is organized as follows. Section II presents the methodology for calculating the module's series resistance from light I–V and dark I–V measurements, as well as proposes a set of new diagnostic parameters calculated from the dark I–V curve. Section III presents experimental results for each of the degradation modes discussed, and showcases how the diagnostic parameters can be used to identify each mode. Section IV discusses the experimental findings and provides a guideline for interpreting the results. Last, section V summarizes and concludes the findings of this paper.

2. IDENTIFYING DEGRADATION MODES FROM LIGHT AND DARK I–V CHARACTERISTICS

2.1. Detecting degradation of the electrical properties of the PV module

Dark I–V characterization is a very accurate tool for determining the electrical parameters of solar cells and modules [32], and it has several advantages over light I–V characterization: it is not affected by variations in the light intensity; it does not require a fast measurement process; and it is not affected by shading or other optical factors that usually create distortions in the light I–V characteristic. These advantages make dark I–V measurements a great candidate for detecting degradation of the PV module's electrical components and solar cells.

Prog. Photovolt: Res. Appl. 2016; **24**:517–532 © 2015 John Wiley & Sons, Ltd.
DOI: 10.1002/pip

When measuring the dark I–V, the maximum current (I_L) can be set as the module's datasheet short-circuit current (I_{sc}), or even higher, because higher dark I–V current leads to better sensitivity in detecting series-resistance losses [32]. I_L must be kept constant between consecutive measurements performed on the same module.

To quantify the degradation of the dark I–V characteristic of the module, analogously to the light I–V curve, we use a dark I–V equivalent for the fill factor (FF_{dark}) calculated as shown in Figure 1 and (1). In this case, $V_{d\text{-}max}$ is the voltage at I_L, and (V_p, I_p) can be determined by translating the dark I–V to the first quadrant, by superposition with I_L; after this, the (V_p, I_p) point is calculated as the maximum power point P_{peak} of the superimposed dark I–V, as in (2):

$$FF_{dark} = \frac{|V_p I_p|}{V_{d-max}\, I_L} \tag{1}$$

$$P_{peak} = |V_p I_p| = \max[V_{dark}(I_L - |I_{dark}|)] \tag{2}$$

FF_{dark}, $V_{d\text{-}max}$, and V_p are generic diagnostic parameters meant to reflect the presence of parasitic resistances or other factors associated with the degradation of the PV module's electrical characteristic. Significant changes in these parameters, excluding temperature effects, will indicate that the electrical properties of the module have degraded/changed; by further analyzing the light and dark I–V, we can identify the causes for the degradation.

2.2. Identifying series-resistance losses

A more specific diagnostic parameter that can accurately quantify the total series resistance of the module is the *light–dark* series resistance ($R_{s\text{-}ld}$), calculated from a light and dark I–V curve, as shown in (3) [19,33]. Here, V_{mp} and I_{mp} are the voltage and current at the maximum power point on the light I–V curve, whereas $V_{d\text{-}mp}$ is the voltage corresponding to $I_{dark} = I_{sc} - I_{mp}$ on the dark I–V curve, as shown in Figure 1:

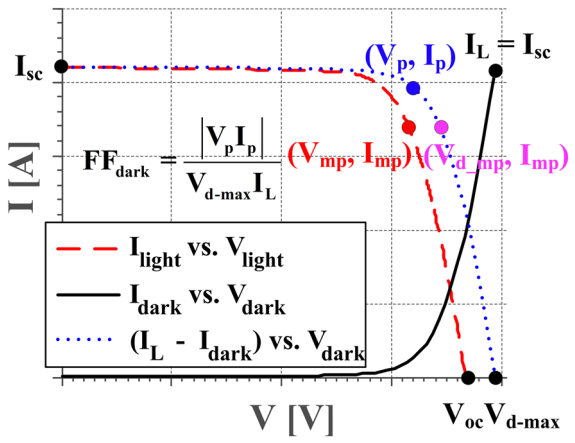

Figure 1. Method for calculating diagnostic parameters (FF_{dark}, $V_{d\text{-}max}$, V_p) from the high voltage/current region of the dark I–V.

$$R_{s-ld} = \frac{V_{d-mp} - V_{mp}}{I_{mp}} \Big| |I_{dark}| = I_{sc} - I_{mp} \tag{3}$$

It is important to mention that both the degradation of the PV module's electrical circuit [18] and mechanical damage to the solar cells [34,35] contribute to increasing the total series resistance of the module; thus, they will be reflected in the $R_{s\text{-}ld}$ and FF_{dark} diagnostic parameters. The two degradation modes can be deconvoluted by considering that degradation of the electrical circuit causes solely resistive losses. In contrast, mechanical damage to the solar cells, leading to cell microcracks and fractures distributed within the PV module, can cause additional shunt [36] and recombination losses [37], which can also be detected in the dark I–V curve. Loss of connected cell area can eventually occur when regions of the metallization grid become open-circuited, reducing photo-generation and causing current mismatch between the cells in the module.

2.3. Proposed method for detecting and identifying shunt and recombination losses

Considering the dark current density–voltage (J–V) characteristic of a crystalline silicon solar cell, shunt and recombination losses, which are associated with leakage currents bypassing the *pn* junction of the solar cell, are most visible in the low/medium voltage region of the dark $ln(J)$–V curve [32,38]. To better illustrate the impact of shunt and recombination losses on the dark J–V characteristic, we simulated the operation of a crystalline solar cell using the well-known two-diode model [32], and the results are shown in Figure 2.

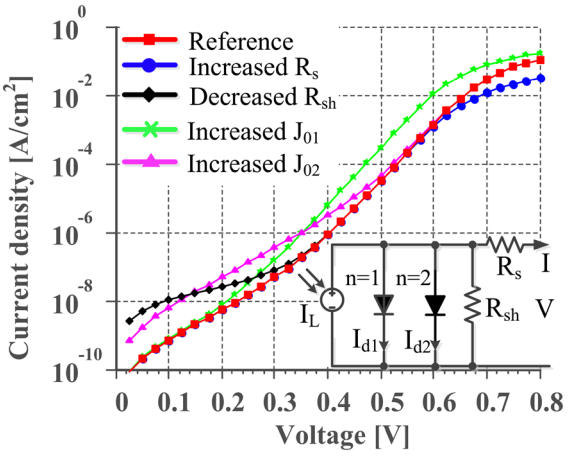

Figure 2. Simulated dark J–V characteristic of a crystalline silicon solar cell affected by different power loss mechanisms (simulated through diode parameter changes): red—reference dark J–V of a solar cell with relatively small series, shunt, and recombination losses ($n_1 = 1$, $n_2 = 2$, $R_s = 0.8\ \Omega cm^2$, $R_{sh} = 10^9\ \Omega cm^2$, $J_{01} = 10^{-13}$ A/cm^2, $J_{02} = 10^{-10}$ A/cm^2); blue—increased $R_s = 4\ \Omega cm^2$; black—decreased $R_{sh} = 10^7\ \Omega cm^2$; green—increased $J_{01} = 10^{-12}$ A/cm^2; magenta—increased $J_{02} = 10^{-9}$ A/cm^2.

The initial parameters of the solar cell were chosen to reflect relatively small shunt, series, and recombination losses, thus yielding the reference dark J–V characteristic shown in Figure 2 (red curve). These parameters are then "degraded" one at a time, to simulate different power loss mechanisms. As observed from Figure 2, shunt losses (R_{sh}) are most visible in the low voltage region of the J–V curve. Increased junction recombination losses (J_{02}) [39] affect both the low and medium voltage regions of the dark J–V, occurring due to the increasing number of defects in the solar cell junction, and have been associated with both cell cracks [37] and PID [38,40]. Losses associated with recombination processes occurring in the surface and bulk of the solar cell (J_{01}) [39] are most visible in the medium and high voltage regions of the J–V. Last, increased resistive losses (R_s) are primarily impacting the high voltage/current regions of the J–V.

The increased shunting (R_{sh}) and recombination losses (J_{01}, J_{02}) show distinct signatures in the low and medium voltage region of the dark $ln(J)$–V. Therefore, analyzing changes in these specific regions can help detect and identify the presence of these degradation mechanisms.

We start from the simplified electrical model of a solar cell without any parasitic resistances (R_s, R_{sh}), as in (4), where J is the current density; V is the terminal voltage; J_0 is the diode saturation current density; n is the diode ideality factor; T is the cell temperature; k is the Boltzmann constant; and q is the elementary charge:

$$J = J_0\left\{\exp\left[\frac{qV}{nkT}\right] - 1\right\} \tag{4}$$

The model can be further simplified by eliminating the "−1" term, which is valid for crystalline silicon cells, where $V >> kT/q$ [41], resulting in a linearized relationship between $ln(J)$ and V, as shown in (5). This simplified model is often used to estimate the saturation current $J_0(V)$ and ideality factor $n(V)$ characteristics of solar cells with low parasitic resistances [41]. Most commonly, the $n(V)$ characteristics have been studied to identify changes in the diode quality factor. Less commonly, the $J_0(V)$ term has been studied. Advantages of studying the $J_0(V)$ term include: (i) it captures changes in both the magnitude of recombination and type of recombination; and (ii) it provides a much more sensitive indicator of all types of changes, increasing both with higher diode quality factor and with parasitic resistance as reflected by a flatter $ln(J)$–V curve. Since this methodology will be applied to modules degrading nonuniformly across the solar cell, instead of a single solar cell, the diode model assumptions may no longer be valid. In this case, to avoid confusion between the voltage-dependent $J_0(V)$ of a solar cell and that of a module, the $J_0(V)$ curve will be denoted hereon as $J_{Loss}(V)$ in the case of modules, and should be interpreted as a diagnostic curve/parameter and not be tied to a specific physical interpretation.

The $J_{Loss}(V)$ characteristic can be calculated by piecewise approximation of the measured $ln(J)$–V curve with equation (5), and solved locally for each (V_k, J_k) measurement point. This can be achieved through curve fitting or by linear approximation, as shown in (6):

$$\ln(J) = \frac{q}{nkt}V + \ln(J_0) \tag{5}$$

$$J_{Loss}(V_k) = J_0(V_k) = \exp\left[\frac{\ln(J_{k-1})V_k - \ln(J_k)V_{k-1}}{V_k - V_{k-1}}\right] \tag{6}$$

The $J_{Loss}(V)$ characteristic, calculated according to (5) and (6), is sensitive to the presence of parasitic resistances and increased recombination processes. This creates a great opportunity for fault detection and identification in solar cells and modules because the onset of failure mechanisms, such as shunting and recombination losses, will be visible in the $J_{Loss}(V)$ curve.

To better exemplify this idea, we apply the $J_{Loss}(V)$ calculation method from (5) and (6) to the simulated dark J–V characteristic of a solar cell impacted by diode parameter changes, as was described in Figure 2. The results presented in Figure 3 for the baseline case reflect the assumed values for J_{02} and J_{01} in the voltage ranges for which each of these dominates. Additionally, Figure 3 data shows that a decreased R_{sh} (black) and increased J_{02} (magenta) losses cause a significant increase in the low voltage area (*Region A*) of the $J_{Loss}(V)$ characteristic. The medium voltage area (*Region B*) of $J_{Loss}(V)$ is impacted by both J_{01} and J_{02}. Last, the high voltage part of region B can also be impacted, to a lesser extent, by increased R_s losses. The quantitative relationships between J_{Loss} and J_{01} and between J_{Loss} and J_{02} are clear. The quantitative relationship between J_{Loss} and shunt or

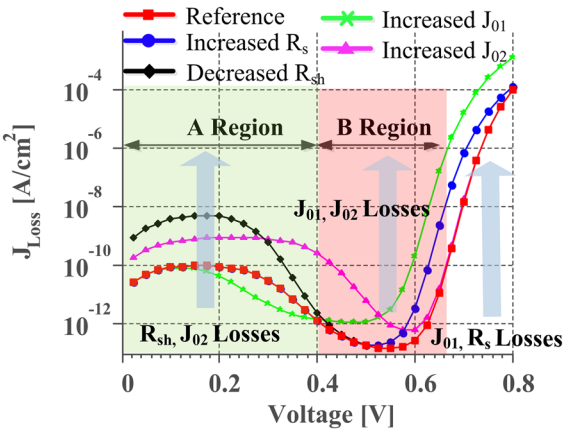

Figure 3. Semilog plot of the $J_{Loss}(V)$ characteristic, calculated from the dark J–V curve of a crystalline silicon solar cell affected by different power loss mechanisms (simulated through diode parameter changes): red—reference dark J–V ($J_{01} = 10^{-13}$ A/cm^2 and $J_{02} = 10^{-10}$ A/cm^2); blue—increased $R_s = 4\ \Omega$cm^2; black—decreased $R_{sh} = 10^7\ \Omega$cm^2; green—increased $J_{01} = 10^{-12}$ A/cm^2; magenta—increased $J_{02} = 10^{-9}$ A/cm^2.

series resistances is less clear, but the strong sensitivity of J_{Loss} to these is readily apparent.

Considering these results, we propose two diagnostic parameters that will indicate the presence of increased shunt and recombination losses. First, $J_{Loss\text{-}A}$ is calculated as shown in (7), and will primarily be sensitive to a decrease in R_{sh} and increased J_{02} losses. Second, $J_{Loss\text{-}B}$, calculated as in (8), will characterize increases in both J_{01} and J_{02} recombination losses, and, to a lesser extent, increased R_s also.

$$J_{Loss-A} = \max[J_{Loss}(V)], for\ 0.1 < V < 0.4 - \text{Reg. A} \quad (7)$$

$$J_{Loss-B} = \min[J_{Loss}(V)], for\ 0.4 < V < 0.66 - \text{Reg. B} \quad (8)$$

These two diagnostic parameters, $J_{Loss\text{-}A}$ and $J_{Loss\text{-}B}$, can be used to identify: (i) cell microcracks and fractures that are known to cause increased series-resistance losses [35], cell shunting [36] and recombination losses [37], as well as (ii) PID, which has been shown to manifest through severe shunting [27,30] and J_{02} losses [38,40], while having a minimal effect on the series resistance of the module [38]. We perform the $J_{Loss}(V)$ analysis in regions A and B wherever the magnitude of change in the curves from initial to degraded condition is largest. However, this position may not be obvious visually on the logarithmic scale.

The dark J–V analysis shown in Figure 3 was performed with a single cell simulation. The extent to which it is valid and will be useful for the diagnostics of modules will be confirmed in the experimental section. Moreover, as previously mentioned, the $J_{Loss}(V)$ curve and the $J_{Loss\text{-}A}$ and $J_{Loss\text{-}B}$ should be interpreted as diagnostic parameters; they should not be tied to a very specific physical interpretation, such as the J_{01} and J_{02} double-diode model parameters obtained through curve fitting the dark J–V. In contrast to curve fitting a diode model, this approach allows for ease of calculation and machine analysis of module dark J–V curves that are degrading nonuniformly across the solar cells, and would lead to curve-fitting problems. This can be the case of modules degrading by PID, where the solar cells closer to the frame degrade faster those in the center, or the case of mechanical degradation of the solar cells.

3. EXPERIMENTAL RESULTS

3.1. Measurement setup

The light I–V characteristic curves of the modules were measured on a class A+A+A+flash tester (Spi-Sun 5600SLP), having a current/voltage measurement accuracy of ±0.2% and an overall repeatability of the STC P_{max}, I_{sc}, V_{oc}, and FF, of less than 0.25%. The dark I–V characteristics of the modules were traced using a Kepco BOP-MG 1KW power supply, and measured using two Keithley 200x digital multimeters with 7-1/2 digit resolution, and a current/voltage measurement accuracy of ±0.005%. The module temperature was measured in both cases using a type K thermocouple, mounted on the backside, with an accuracy of ±0.3 °C.

3.2. Optical losses

Optical losses can have various effects on the light I–V characteristic of the module and can be difficult to quantify or identify without additional diagnostic measurements or visual inspection. For modules with bypass diodes, we can generally categorize the impact on the light I–V as *homogenous/uniform*, characterized by a reduction in light reaching the solar cells; and a *heterogeneous/partial* impact on the light I–V due to the activation of bypass diodes (assumed to be functioning in this analysis) and the presence of inflection points in the I–V curve.

We reproduced these two effects on a 72 cell multicrystalline silicon PV module with four bypass diodes by covering parts of the module with semi-transparent foils. In the first experiment, we covered the entire module with one layer of semi-transparent foil, resulting in a uniform shading of the module. In the next two experiments, we covered only two cells of the module, once with two layers of semi-transparent foil, and once with four layers of foil, emulating partial shading on the module. Afterwards, we measured the light I–V characteristic under *Standard Test Conditions* (STC—1000 W/m^2, 25 °C, AM 1.5) on a solar simulator. The resulting light I–V curves, normalized in voltage on a per-cell basis, are presented in Figure 4, where the partial and uniform effects are illustrated.

As observed from Figure 4 and Figure 5, *partial shading* can lead to a significant decrease in fill factor and to the

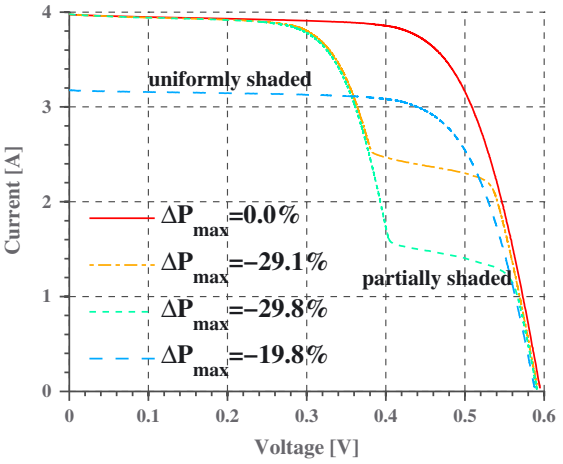

Figure 4. Light I–V characteristic of a crystalline silicon PV module with bypass diodes, affected by uniform shading (blue curve)—where the entire module covered with one layer of semi-transparent foil; and by partial shading—where only two cells were covered once with two layers of foil (orange curve), and once with four layers of foil (green curve). The module I–V curves are normalized in voltage to a per-cell basis.

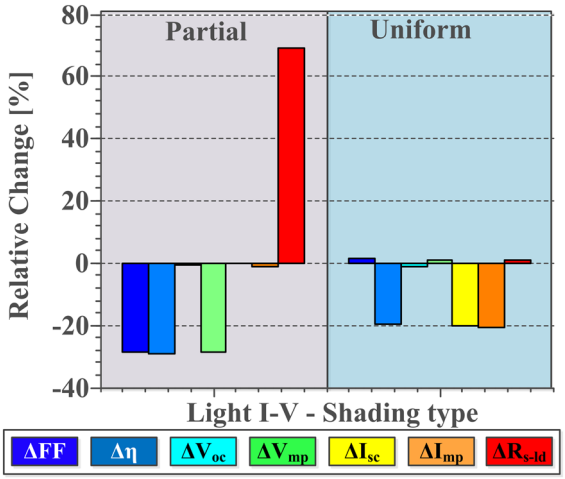

Figure 5. Effects of partial (two cells covered with two layers of semi-transparent foil) and uniform (100% module area covered with a single layer of foil) shading on the light I–V parameters of a PV module with bypass diodes. The initial STC I–V parameters of the module were $FF_0 = 0.70$, $\eta_0 = 10.95\%$, $V_{oc0} = 42.87$ V, $V_{mp0} = 33.21$ V, $I_{sc0} = 3.97$ A, $I_{mp0} = 3.62$ A, and $R_{s\text{-}ld0} = 1.82\ \Omega\text{cm}^2$.

creation of multiple maximum power points, which is especially misleading for the maximum power tracker of the converter. Attention must be given to avoid confusing this signature, as shown in Figure 5, with the series resistance of a module, where the $R_{s\text{-}ld}$ parameter shows a false increase due to the inflection point in the light I–V.

Similarly, *uniform shading* leads to a decrease in current generation (I_{sc}, I_{mp}), but does not have a proportional impact on the fill factor. This case can be difficult to detect from the light I–V alone without measuring the irradiance and module temperature conditions, as well.

Measurement of the dark I–V curve parameters are not influenced by optical losses. If no significant changes are detected (excluding temperature effects), we can conclude that the degradation mode is of optical nature and appropriate maintenance actions can be performed.

3.3. Degradation of the electrical circuit of the PV module

To reproduce this failure mode, we impaired increasing levels of damage to the cell interconnect ribbons of four conventional 60 cell multicrystalline silicon PV modules (denoted R1 to R4), glass front cover, ethylene-vinyl-acetate (EVA) encapsulant, and Tedlar backsheet. In module R1, two out of three ribbons per cell (for a total of four cells) were cut from the backside of the module, causing a 1.7% degradation of the STC maximum power of the module (Figure 6). Modules R2, R3, and R4 sustained increasing numbers of damaged cells (12, 16, and 24) interconnects leading to additional power loss, as shown in Table I.

The four modules were characterized before and after impairing the damage by light I–V measurements at STC

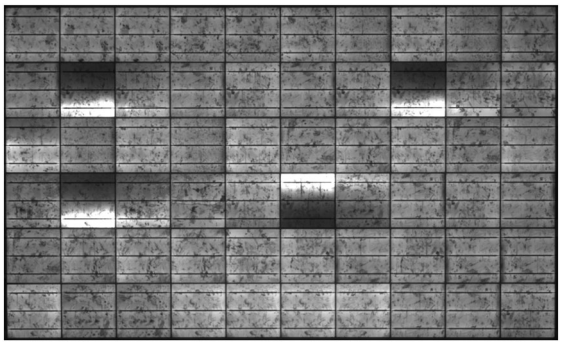

Figure 6. Electroluminescence image of module R1 taken at STC I_{mp} bias. The module sustained open-circuited cell interconnects, causing 1.7% STC P_{max} loss.

Table I. Relative change in the light I–V parameters (measured at STC) of the four PV modules that have sustained different levels of damage to their cell interconnects.

Module	R1	R2	R3	R4
P_{max0} [W]	246.02	233.2	234.8	237.5
ΔP_{max} [%]	−1.7	−3.1	−5.5	−.4
FF_0	0.752	0.745	0.744	0.744
ΔFF[%]	−1.84	−2.74	−5.18	−6.1
η_0 [%]	15.15	14.36	14.46	14.63
$\Delta\eta$ [%]	−1.72	−3.13	−5.5	−6.27
V_{oc0} [V]	37.3	36.9	37.07	37.16
ΔV_{oc} [%]	0.04	−0.04	−0.03	0.04
V_{mp0} [V]	29.86	29.39	29.58	29.72
ΔV_{mp} [%]	−1.41	−2.7	−4.53	−4.82
I_{sc0} [A]	8.76	8.47	8.5	8.58
ΔI_{sc} [%]	0.09	−0.3	−0.27	−0.29
I_{mp0} [A]	8.24	7.93	7.93	7.99
ΔI_{mp} [%]	−0.31	−1.08	−1.02	−1.54

as well as dark I–V measurements (25 °C), which are summarized in Table I and Table II.

By analyzing the relative change in the STC light I–V parameters from Table I, we observe a proportional decrease in *FF* and module efficiency (η), which is mainly attributed to an increased voltage drop in the V_{mp} region of the I–V curve. Furthermore, the I_{sc} and V_{oc} remain virtually

Table II. Relative change in the dark I–V parameters of the four PV modules that have sustained different levels of damage to their cell interconnects.

Module	R1	R2	R3	R4
ΔP_{max} [%]	**−1.7**	**−3.1**	**−5.5**	**−6.3**
ΔFF_{dark} [%]	−0.84	−1.06	−1.95	−2.77
$\Delta V_{d\text{-}max}$ [%]	1.04	1.76	2.88	3.84
ΔV_p [%]	0.02	−0.14	1.24	1.18
$\Delta R_{s\text{-}ld}$ [%]	22.4	38.2	65.8	76.2
$\Delta J_{Loss\text{-}B}$ [%]	12.9	10.76	32.1	25.9
$\Delta J_{Loss\text{-}A}$ [%]	−10.4	−30	−11.8	−27.8

unchanged, considering a measurement uncertainty of ±0.25%, implying that the power loss is of purely resistive nature, although a very large increase in series resistance (typical values are from 0.8 to 10 Ωcm^2) [42] would lead to a decrease in I_{sc}, but not in the V_{oc}.

Next, if we analyze the light performance of module R1 (Figure 7), for example, we can observe that the damage to the cell interconnects causes a small increase in the module's external series resistance, which is visible only under high illumination.

This effect is better illustrated by calculating the relative change in the light I–V parameters, as in Figure 8. From here, it can be observed that the decrease in *FF*, η, and V_{mp} is more pronounced at higher light intensity, due to the additional voltage drop caused by the increased series resistance. Similar changes in the light performance characteristic of a module can be used to confirm the presence of increased series-resistance losses, versus other mechanisms, such as shunting, that have an opposite behavior, as will be shown in the next sections.

In the case of dark I–V measurements, increases in the external series resistance are visible in the high current region of the dark I–V (Figure 9), causing an increase in voltage ($V_{d\text{-}max}$) due to the additional voltage drop.

This failure mode is best characterized by the $R_{s\text{-}ld}$ parameter, which combines both the light and dark I–V characteristics, and it is most sensitive to increased series-resistance losses. For example, in the case of module R1, which experiences only 1.7% power loss due to open-circuited cell interconnects, the $R_{s\text{-}ld}$ increases by 22.4%.

Further analysis of the low and medium voltage regions of the dark I–V in Figure 9 does not reveal any additional power loss mechanisms. This is confirmed in Figure 10 by calculating the $J_{Loss}(V)$ characteristic for the worst degraded module (R4) and the highest increase in series resistance. Here, we observe that changes in the $J_{Loss}(V)$ curve are minor. These findings agree with our expectations because degradation of the electrical circuit is not associated with shunting or recombination processes, which would have a significant impact on this curve.

The relative change in dark I–V parameters due to open-circuited cell interconnects is summarized in Table II for all four modules. Here, we observe that this particular failure mode is reflected mainly by a significant increase in $R_{s\text{-}ld}$, followed by a smaller increase in $V_{d\text{-}max}$ (the dark

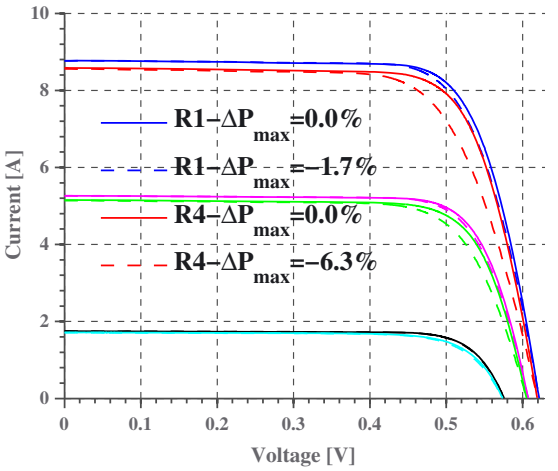

Figure 7. Light I–V characteristic of modules R1 and R4 with open-circuited cell interconnects (full lines – no damage; dashed lines—after damage), causing 1.7% and 6.4% STC P_{max} loss, respectively. The I–V curves were measured at 1000 (blue—R1, red—R4), 600 (magenta—R1, green—R4), and 200 (black—R1, green—R4) W/m^2 and 25 °C. The module I–V curves are normalized in voltage on a per-cell basis.

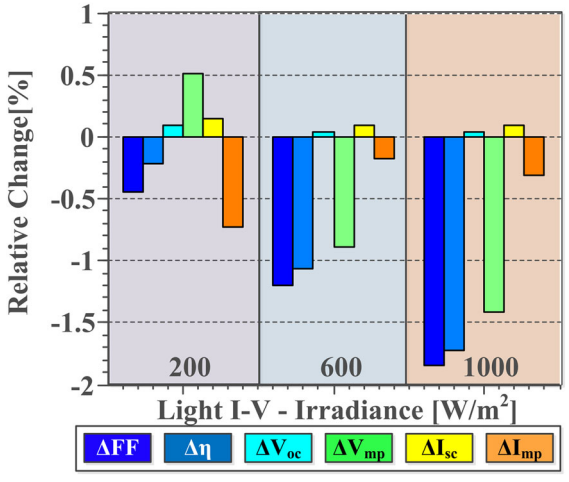

Figure 8. Relative change in light I–V parameters (measured at 1000, 600, and 200 W/m^2 and 25 °C) of module R1 with open-circuited cell interconnects, causing 1.7% STC P_{max} loss.

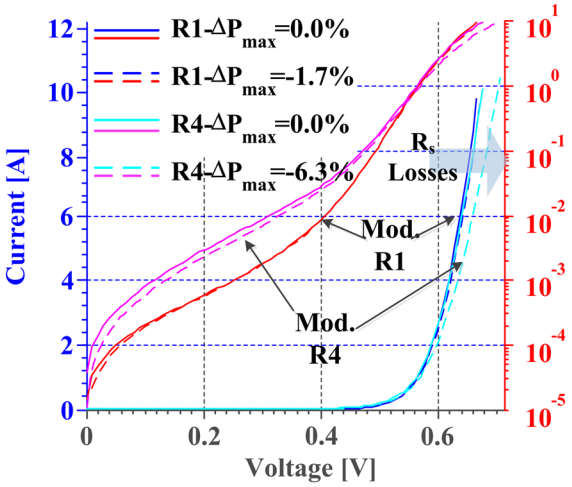

Figure 9. Dark I–V characteristic of modules R1 and R4 with open-circuited cell interconnects (full lines—no damage; dashed lines—after damage), causing 1.7% and 6.3% STC P_{max} loss, respectively. The dark I–V curves were measured at 25 °C and are plotted in linear (blue—R1, cyan—R4) and log scales (red—R1, magenta—R4). The module I–V curves are normalized in voltage on a per-cell basis.

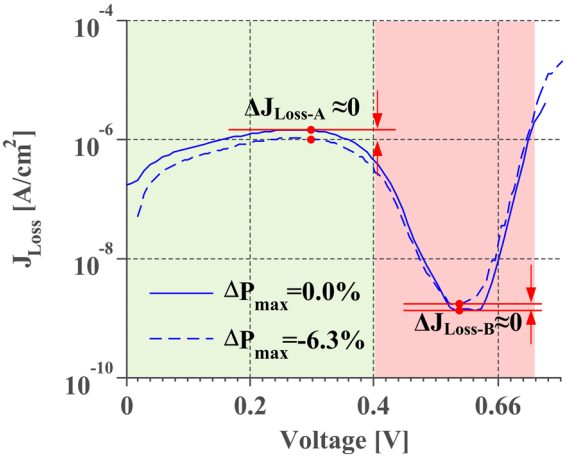

Figure 10. Semilog plot of the J_{Loss}(V) characteristic of module R4 with open-circuited cell interconnects (full lines—no damage; dashed lines—after damage), causing 6.3% STC P_{max} loss.

I–V voltage at I_L), as well as a decrease of FF_{dark}, suggesting additional electrical losses occurring in the module.

In the case of the $J_{Loss\text{-}A}$ and $J_{Loss\text{-}B}$ parameters, we can see a relatively small variation (compared to the other failure types), which is mostly due to temperature variations and numerical noise. Previously repeat measurements on another module design yielded a compound uncertainty of ±8% for these two parameters, for a ±0.8 °C uncertainty in the module temperature. Considering this, the change in $J_{Loss\text{-}A}$ and $J_{Loss\text{-}B}$ is not significant enough to be attributed to any shunting or recombination losses, which will become more evident in the following sections.

3.4. Mechanical damage to the solar cells

This degradation mode was reproduced in a laboratory environment by mechanically loading the PV modules and expanding the microcracks by exposing them to humidity-freeze cycles according to IEC 61215. We applied this accelerated procedure to a conventional 60 cell multicrystalline silicon PV module, with glass front cover, EVA encapsulant, and Tedlar backsheet. The module was stressed and characterized for a total of three rounds, resulting in a gradual mechanical degradation of the solar cells, as shown in Figure 11.

After initial characterization, the module entered the first stress round (b), where it was loaded with ~400 kg of sandbags, after which it underwent twenty-two humidity–freeze stress cycles in the environmental chamber. After I–V and electroluminescence characterization, the module underwent the second stress round (c), consisting of additional mechanical loading. In the third stress round (d), the module underwent thirteen more humidity–freeze cycles, before final characterization.

By analyzing the light I–V measurements (1000, 600, and 200 W/m^2 and 25 °C) acquired before, during, and after the stress procedure, as displayed in Figure 12, we can observe a P_{max} degradation occurring at both high and low illumination conditions.

The relative change in the light I–V parameters of the module is shown in Figure 13 for the first stage of

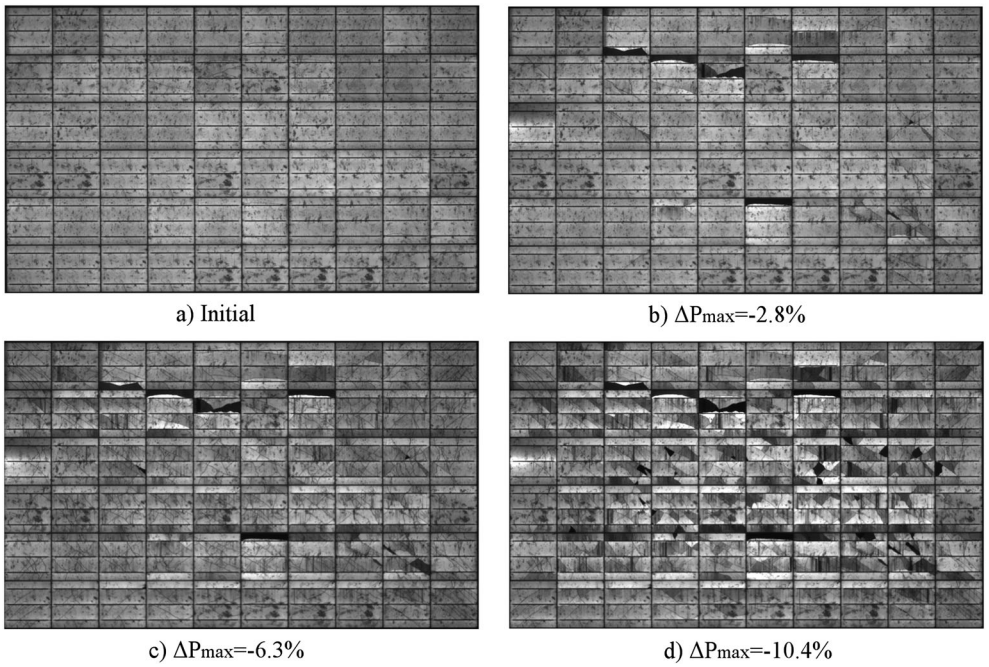

Figure 11. Electroluminescence image of a crystalline silicon PV module taken at STC I_{mp} bias. The module has sustained three rounds of mechanical damage to its cells. The module's STC P_{max} degraded with: a) initial—no degradation b) −2.8%; c) −6.3%; d) −10.4%.

DOI: 10.1002/pip

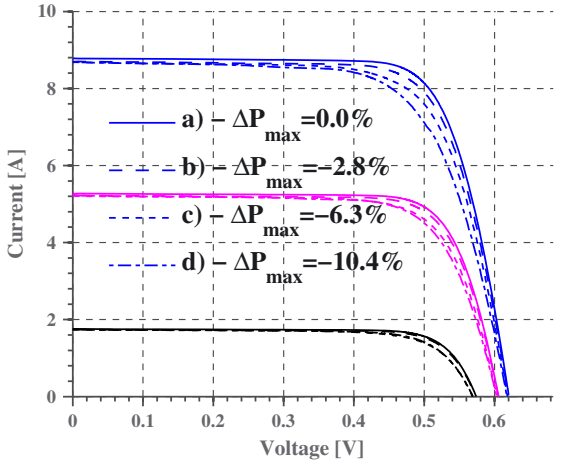

Figure 12. Light I–V characteristic of a PV module with mechanically damaged solar cells, causing 2.8%, 6.3%, and 10.4% STC P_{max} loss, respectively. The I–V curves were measured at 1000 (blue), 600 (magenta), and 200 (black) W/m^2 and 25 °C. The module I–V curves are normalized in voltage on a per-cell basis.

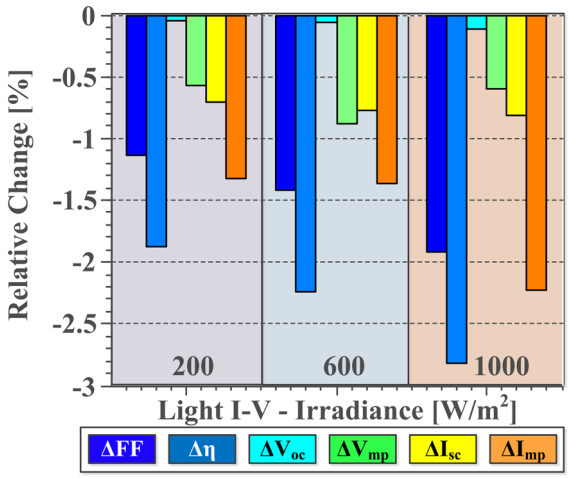

Figure 13. Relative change in the light I–V parameters (measured at 1000, 600, and 200 W/m^2 and 25 °C) of a PV module with mechanically damaged solar cells (after the first damage event), causing 2.8% STC P_{max} loss.

degradation of the module (2.8% STC power loss), where we observe a similar degradation in the STC and the low light efficiency, as well as reduction in current generation (I_{sc}), most probably due to the cell fractures and removal of cell pieces from the cell circuit.

If we analyze the relative change in the STC light I–V parameters over the degradation of the module, as presented in Table III, we can observe a significant I_{mp} current loss, which in some cases is greater than the V_{mp} voltage loss, suggesting: loss of well-connected cell area, shunting, J_{02} losses, and cell mismatch taking place in addition to series resistance losses [14], unlike the previous case of ribbon open-circuits. Moreover, we can see a V_{oc} degradation that could be explained by J_{01} losses or internal short circuits. This case contrasts with increased external series resistance, where V_{mp} voltage losses are dominant, while the V_{oc} remains unchanged.

Table III. Relative change in the light I–V parameters (measured at STC) of a PV module, presented in different stages of mechanical degradation of its solar cells.

Damage	b	c	d
P_{max0} [W]		244.43	
ΔP_{max} [%]	−2.8	−6.3	−10.4
FF_0		0.749	
ΔFF[%]	−1.9	−5.08	−9.18
η		15.05	
Δη [%]	−2.8	−6.33	−10.4
V_{oc0} [V]		37.21	
ΔV_{oc} [%]	−0.11	−0.26	−0.41
V_{mp0} [V]		29.67	
ΔV_{mp} [%]	−0.6	−1.42	−5.64
I_{sc0} [A]		8.77	
ΔI_{sc} [%]	−0.8	−1.05	−0.95
I_{mp0} [V]		8.24	
ΔI_{mp} [%]	−2.22	−4.97	−5.05

The dark I–V characteristics of the module, shown in Figure 14, confirm the increased series-resistance losses, characterized by an increased $V_{d\text{-}max}$, as well as shunting and recombination losses visible in the low voltage region of the dark I–V.

Further investigation of the $J_{Loss}(V)$ curve, shown in Figure 15, confirms increased saturation currents in both the J_{01} and J_{02} regions, although the extent of their increase

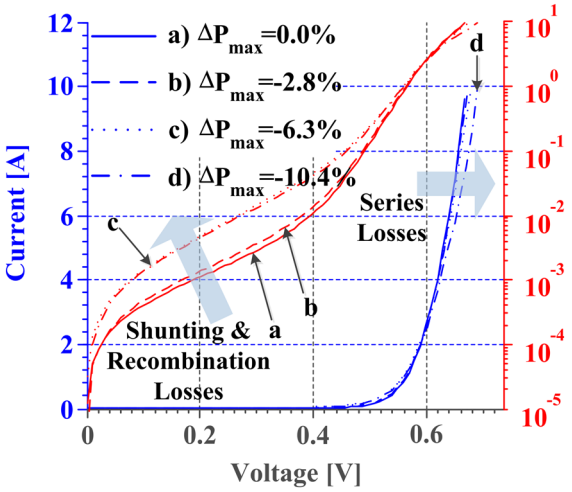

Figure 14. Dark I–V characteristic of a PV module with mechanically damaged solar cells (full lines—no damage; dashed lines—after damage during three events), causing 2.8%, 6.3%, and 10.4% STC P_{max} loss, respectively. The dark I–V curves were measured at 25 °C and are plotted in linear (blue) and log scales (red). The module I–V curves are normalized in voltage on a per-cell basis.

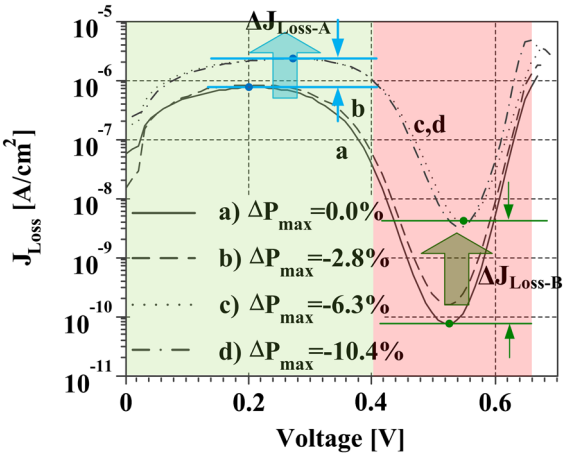

Figure 15. Semilog plot of the J_{Loss}(V) characteristic of a PV module with mechanically damaged solar cells (full lines—no damage; dashed lines—after damage during three events), causing 2.8%, 6.3%, and 10.4% STC P_{max} loss, respectively.

varies with each degradation/stress stage sustained by the module.

The first stress stage results in a 2.8% STC power drop due to several cell microcracks and fractures sustained by the module (Figure 11b). This is reflected by a 17.8% increase in series resistance ($R_{s\text{-}ld}$) and a 117.5% increase in $J_{Loss\text{-}B}$, as shown in Table IV, suggesting increased series and recombination losses.

After the second stress stage (Figure 11c), the number of cracked cells increases considerably, whereas the fracture cell area increases only slightly. In this situation, we observe a significant increase in $J_{Loss\text{-}B}$ (>50 times) and $J_{Loss\text{-}A}$ (more than two-fold) compared to $R_{s\text{-}ld}$ (37.9%), suggesting as previously shown in Figure 3, active shunting and recombination losses in addition to series resistance. Moreover, J_{02} and shunt losses, reflected in the $J_{Loss\text{-}A}$ parameter, have strong influence on low-light performance of the module, as shown in Figure 13, and can also influence one-sun performance as degradation progresses, as observed in Figure 12.

Additional stress leads to an increased number of fractured/inactive cell areas, as observed in Figure 11d. The additional power loss may mostly be caused by series resistance ($R_{s\text{-}ld}$), which almost doubles, because $J_{Loss\text{-}A}$ and $J_{Loss\text{-}B}$ do not increase any further. This is confirmed by a significant decrease in V_{mp} compared to the previous stress stage (from −1.41% to −5.64%) as well as increased $V_{d\text{-}max}$ (2.9%), which also suggests resistive losses.

If we combine the results regarding the light performance of the module (Figure 13) with the relative variation of the light I–V (Table III) and dark I–V (Table IV) parameters, we can conclude that mechanical damage to the solar cells results in: (i) increased series-resistance losses (visible by $R_{s\text{-}ld}$ and $V_{d\text{-}max}$); (ii) increased shunting and recombination losses ($J_{Loss\text{-}A}$ and $J_{Loss\text{-}B}$); (iii) degradation of both STC and low light efficiency; (iv) decreased current generation (I_{sc}); (v) large I_{mp} current losses; and (vi) general degradation of the solar cell's electrical characteristic/parameters (FF_{dark}).

Table IV. Relative change in the dark I–V parameters of a PV module, presented in different stages of mechanical degradation.

Damage	b	c	d
ΔP_{max} [%]	−2.8	−6.3	−10.4
ΔFF_{dark} [%]	−0.8	−2.7	−4.3
$\Delta V_{d\text{-}max}$ [%]	0.3	1	2.9
ΔV_p [%]	−1.8	−1.8	−1.8
$\Delta R_{s\text{-}ld}$ [%]	17.8	37.9	87.6
$\Delta J_{Loss\text{-}B}$ [%]	1E2	51E2	44E2
$\Delta J_{Loss\text{-}A}$ [%]	1E1	2E2	2E2

3.5. Potential-induced degradation

PID can be reproduced in the laboratory by means of damp-heat stress testing with applied system voltage bias [43]. We performed such an accelerated PID stress test on four conventional 60 cell multicrystalline silicon modules of different designs and PID sensitivity levels, with standard aluminum frame, EVA encapsulant, tempered front glass cover, and Tedlar backsheet. Modules P1, P3, and P4 were stressed at 60 °C/85% relative humidity (RH) and −1000 V bias, during which they exhibited medium to high PID sensitivity. The fast degradation rate of these modules is readily evident from the *STC* P_{max} degradation curves shown in Figure 16, measured in situ according to the procedure described in [44]. In contrast, module P2, which was designed by the manufacturer to be PID-resistant, degraded much slower, as can be observed from Figure 16.

The performance of the four modules was characterized on a solar simulator at STC, before and after PID stress test. Looking at the relative change in STC light I–V parameters in Table V, we observe a pronounced I_{mp} current

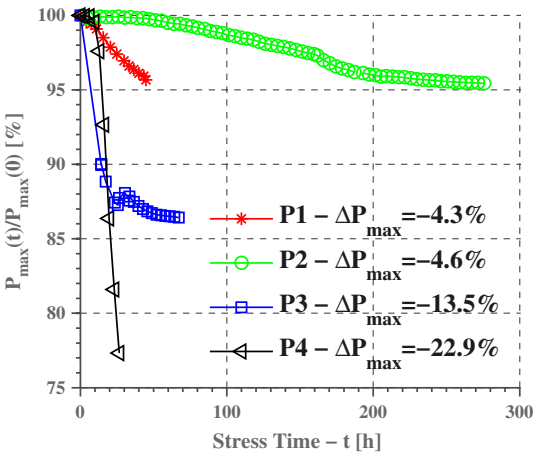

Figure 16. STC P_{max} degradation curves of the four modules affected by PID, as a function of stress time. The degradation curves were determined from in situ dark I–V measurements.

Table V. Relative change in the light I–V parameters (measured at STC) of the four PV modules affected by PID.

Module	P1	P2	P3	P4
P_{max0} [W]	242.57	249.5	236.43	224.55
ΔP_{max} [%]	−4.3	−4.6	−13.5	−22.9
FF_0	0.737	0.76	0.736	0.747
ΔFF [%]	−3.82	−4.04	−12.25	−18.2
η_0 [%]	14.94	16.1	14.56	13.83
$\Delta\eta$ [%]	−4.34	−4.35	−13.5	−22.3
V_{oc0} [V]	37.26	37.73	37.11	36.16
ΔV_{oc} [%]	−0.36	−0.34	−1.24	−6.05
V_{mp0} [V]	29.45	30.77	29.59	29.05
ΔV_{mp} [%]	1.25	−1.07	−5.62	−14.8
I_{sc0} [A]	8.82	8.69	8.65	8.3
ΔI_{sc} [%]	−0.17	−0.24	−0.17	0.4
I_{mp0} [A]	8.23	8.1	7.99	7.73
ΔI_{mp} [%]	−5.51	−3.59	−8.33	−9.5

loss and *FF* degradation commonly associated with PID. Interestingly, V_{oc} and V_{mp} voltage losses are small for modules P1 and P2, which degraded only about 4.5% due to PID, whereas modules P3 and P4 show more significant voltage losses. These additional voltage losses could be explained by increased J_{01} and/or a decrease in R_{sh}. One important fact to notice from Table V is that the current generation (I_{sc}) is not significantly affected by PID, even for relatively large extents of degradation; this is consistent with similar findings in the literature [27,30,31]. However, this can change if R_{sh} is drastically reduced, which can be the case in highly PID-sensitive modules [27,29,30].

Further analysis of the multi-light I–V characteristic of module P1 in Figure 17 reveals a stronger degradation of the module's low light performance compared with higher light-intensity levels. This reduction in performance is explained by additional voltage losses (V_{oc}, V_{mp}) occurring under low light conditions (Figure 18), which are consistent with shunting.

The four modules were characterized in situ, by periodically (every 3 h) ramping down the chamber from the stress temperature of 60 °C down to 25 °C and measuring the modules' dark I–V characteristic, as described in [43]. Figure 19 illustrates the gradual degradation of module P1 over the course of the PID stress test. Here, we can observe a mixed recombination loss mechanism. The initial stages of degradation occur in the low voltage region

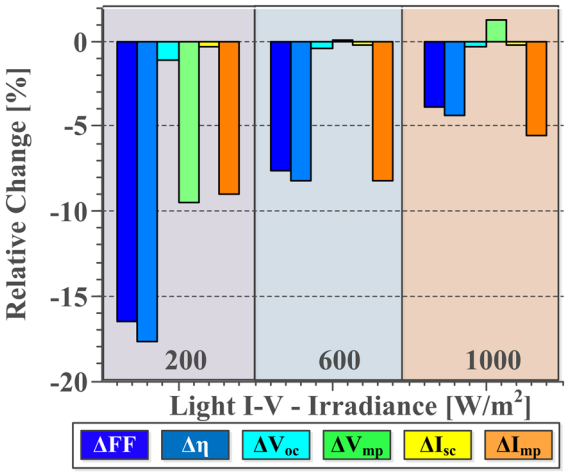

Figure 18. Relative change in the light I–V parameters (measured at 1000, 600, and 200 W/m^2 and 25 °C) of module P1 experiencing 4.3% STC P_{max} loss due to PID.

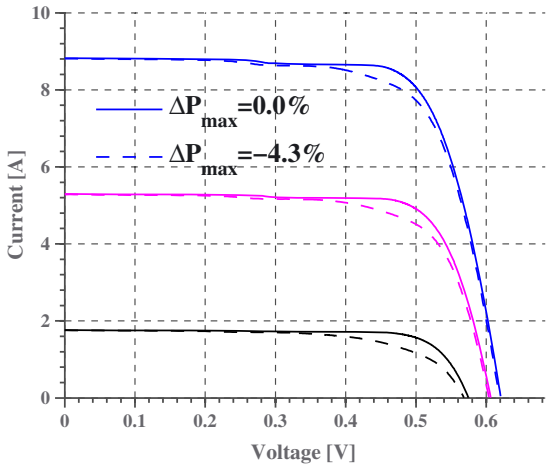

Figure 17. Light I–V characteristic of module P1 (full lines—no PID; dashed lines—after PID), causing 4.3% STC P_{max} loss. The I–V curves were measured at 1000 (blue), 600 (magenta), and 200 (black) W/m^2 and 25 °C. The module I–V curves are normalized in voltage on a per-cell basis.

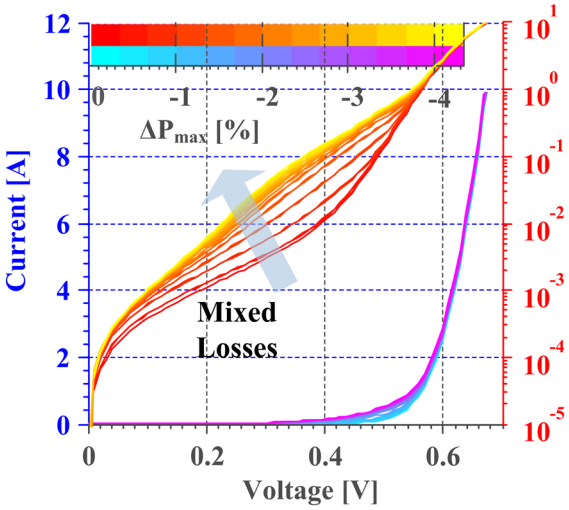

Figure 19. Dark I–V characteristics of module P1 (cyan—no PID; magenta—after PID), causing 4.3% STC P_{max} loss. The dark I–V curves were measured in situ at 25 °C, during the accelerated PID stress test. The module I–V curves are normalized in voltage on a per-cell basis.

of the I–V, associated with J_{02} losses, which are gradually dominated by degradation occurring in the medium voltage region. This degradation mechanism is difficult to deconvolute by a simple two-diode model approach because we are analyzing the I–V characteristic of a PV module consisting of 60 cells that degrade at different rates, depending on their relative position to the module frame.

A similar degradation dynamic is observed in the $J_{Loss}(V)$ curve in Figure 20, which is characterized by an initial increase in $J_{Loss\text{-}A}$ that is surpassed by a very large increase in $J_{Loss\text{-}B}$ in the later stages of degradation. At the end of the stress test, when module P1 degraded by only 4.3% (STC power loss), the relative change in dark I–V parameters in Table VI shows that parameter $J_{Loss\text{-}B}$ increased more than 400 fold whereas $J_{Loss\text{-}A}$ increased over 8 times from its original value, although the series resistance remained practically unchanged.

Similar PID signatures were found for modules P3 and P4 (summarized in Table VI), which could be explained by the high susceptibility of these module to PID.

By comparison, module P2, which was the least sensitive to PID, shows a dominant J_{02} recombination mechanism (Figure 21), consistent with similar results in the literature [38,40]. In addition, the $J_{Loss}(V)$ characteristic in Figure 22 shows a significant increase in $J_{Loss\text{-}A}$ (~16 times), consistent with R_{sh} and J_{02} losses. However, $J_{Loss\text{-}B}$ shows a lower increase (~52 times) compared to the other three modules, due to the dominant shunting and J_{02} loss mechanisms.

The relative change in dark I–V parameters, summarized in Table VI, reveals more PID-specific signatures that can be used to identify this particular failure mode. The onset of PID is reflected in a significant decrease in FF_{dark}—much more than for the other investigated failure modes—confirming the prominent FF degradation mechanism. However, the series resistance of the module ($R_{s\text{-}ld}$) does not increase significantly, even for the worst degraded module. This aspect can

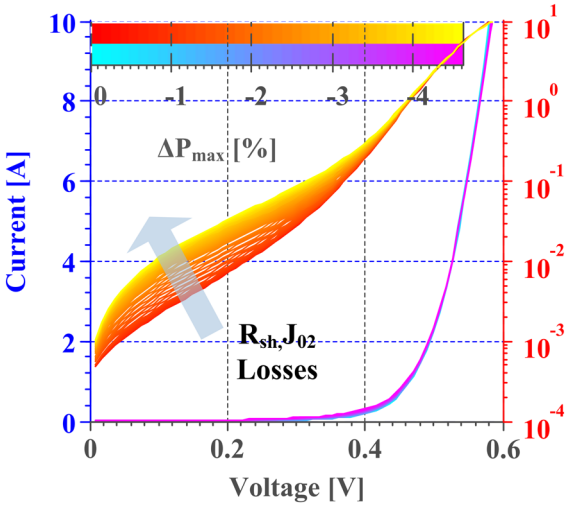

Figure 21. Dark I–V characteristics of module P2 (cyan—no PID; magenta—after PID), causing 4.6% STC P_{max} loss. The dark I–V curves were measured in situ at stress temperature, during the accelerated PID stress test. The module I–V curves are normalized in voltage on a per-cell basis.

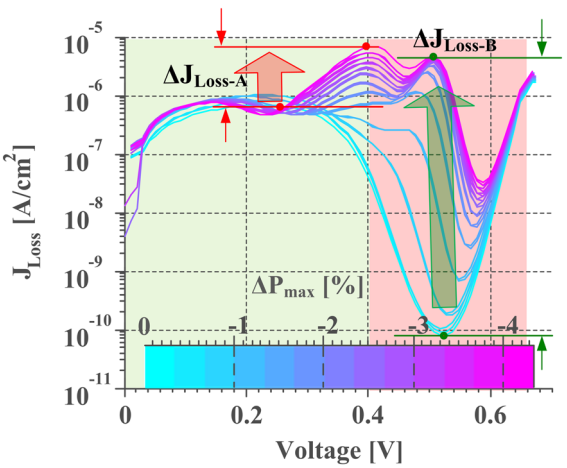

Figure 20. Semilog plot of the $J_{Loss}(V)$ characteristics of module P1 (cyan—no PID; magenta—after PID) causing 4.3% STC P_{max} loss, calculated from the dark I–V curves measured in situ at 25 °C, during the accelerated PID stress test.

Table VI. Relative change in the dark I–V parameters of the four PV modules affected by PID.

Module	P1	P2	P3	P4
ΔP_{max} [%]	−4.3	−4.6	−13.5	−22.9
ΔFF_{dark}[%]	−4.05	−3.86	−11.6	−17.1
$\Delta V_{d\text{-}max}$ [%]	−0.6	0.45	−1.13	−5.3
ΔV_p [%]	−0.01	0.01	−3.84	−15.3
$\Delta R_{s\text{-}ld}$ [%]	−2.9	3	3.56	9.2
$\Delta J_{Loss\text{-}B}$ [%]	4.1E4	5.2E3	5.2E5	9.9E5
$\Delta J_{Loss\text{-}A}$ [%]	8.5E2	1.6E3	5E1	4.5E2

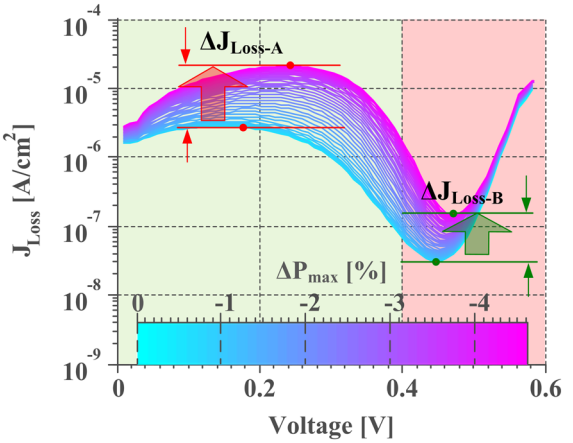

Figure 22. Semilog plot of the $J_{Loss}(V)$ characteristics of module P2 (cyan—no PID; magenta—after PID) causing 4.6% STC P_{max} loss, calculated from the dark I–V curves were measured in situ at stress temperature, during the accelerated PID stress test.

Table VII. Effect of different degradation modes on the light I–V and dark I–V parameters.

	Light I–V*					Dark I–V*				
Degradation mode	FF	FF (low light)	I_{sc}	V_{oc}	$\Delta R_{s\text{-}ld}$	FF_{dark}	$V_{d\text{-}max}$	V_p	$J_{Loss\text{-}B}$	$J_{Loss\text{-}A}$
Optical loss	↓↑	↓↑	↓	↓	↓↑	0	0	0	0	0
Electrical loss	↓↓	↓	↓	0	↑↑	↓↓	↑	↑	0	0
Cell damage	↓	↓	↓	↓	↑↑	↓	↑	↓	↑↑↑	↑↑
PID	↓↓	↓↓↓	0	↓	0	↓↓	↓↓	↓	↑↑↑↑	↑↑↑

*Legend: ↓↑—inconsistent variation; ↓—small decrease; ↓↓—substantial decrease; ↓↓↓—large decrease; 0—no significant change; ↑—small increase; ↑↑—substantial increase; ↑↑↑—large increase; ↑↑↑↑—very large increase.

be used to exclude degradation of the modules electrical circuit or mechanical damage as the dominant failure mode.

From Table VI, it can be observed that for modules with pronounced PID, such as P3 and P4, $V_{d\text{-}max}$ and V_p show a significant decrease. This contrasts with other degradation modes characterized by increased series-resistance losses, which would lead to an increase in $V_{d\text{-}max}$ and possibly V_p due to the additional voltage drop generated by the increased series resistance.

Perhaps the most significant parameters for identifying the presence of PID are $J_{Loss\text{-}A}$ and $J_{Loss\text{-}B}$, which show a very large increase for this particular failure mode, as can be observed in Table VI—several orders of magnitude larger than in the case of cell microcracks and fractures (Table IV).

4. DISCUSSION

The four degradation modes discussed in this article have different signatures reflected on the light I–V (FF, I_{sc}, V_{oc}, V_{mp}, $R_{s\text{-}ld}$) and dark I–V (FF_{dark}, $V_{d\text{-}max}$, V_p, $J_{Loss\text{-}A}$, $J_{Loss\text{-}B}$) diagnostic parameters, as shown in Table VII. These signatures can be used to devise a simple fault-identification procedure summarized as follows:

- Changes in light I–V parameters (FF, I_{sc}, $R_{s\text{-}ld}$) but not present in the dark I–V parameters (FF_{dark}, $V_{d\text{-}max}$, V_p) indicate optical losses.
- Mixed degradation modes, such as delamination, can first occur as inconsistencies between the light and dark I–V, being identified as optical losses. But if this is left unchecked it can also lead to degradation of the solar cells, and/or the electrical circuit of the module. This would ultimately impact the dark I–V characteristic, and signal an electrical/material issue with the module. In this case, monitoring the history of the light I–V and dark I–V parameters changes would help identify this type of degradation occurring.
- Increased $R_{s\text{-}ld}$, decreased FF, near-constant V_{oc}, and small or no decrease in low light performance accompanied by a decrease in FF_{dark}, increased $V_{d\text{-}max}$, and near-constant $J_{Loss\text{-}A}$ and $J_{Loss\text{-}B}$ indicate increased external series resistance due to the degradation of the PV module's electrical circuit.
- Increased $R_{s\text{-}ld}$, decreased FF, possible decrease in I_{sc} and V_{oc}, and medium decrease in low light performance accompanied by a decrease in FF_{dark}, increased $V_{d\text{-}max}$, and a significant increase in $J_{Loss\text{-}A}$ and $J_{Loss\text{-}B}$ indicate mechanical damage of the solar cells.
- Decrease in FF and possibly V_{oc}, near-constant $R_{s\text{-}ld}$ and I_{sc}, a significant decrease in low light performance accompanied by a decrease in FF_{dark}, possible decrease $V_{d\text{-}max}$, and a very large increase in $J_{Loss\text{-}A}$ and $J_{Loss\text{-}B}$ indicate the onset of PID.

The calculation and analysis of the diagnostic parameters (FF, I_{sc}, V_{oc}, V_{mp}, $R_{s\text{-}ld}$, FF_{dark}, $V_{d\text{-}max}$, V_p, $J_{Loss\text{-}A}$, and $J_{Loss\text{-}B}$) involved in the fault-identification process can be automated and integrated into the light I–V and dark I–V measurement hardware—whether it be an I–V tracer, module-integrated converter, inverter, or other hardware capable of measuring the light and dark I–V characteristic. Special considerations must be taken of the ambient conditions (light intensity and module temperature) during the I–V measurement process so as not to introduce large measurement errors into the diagnostic parameters.

5. SUMMARY AND CONCLUSION

The current work proposed a fault-identification method for identifying four important degradation modes that lead to power loss in PV modules: (i) degradation of the electrical circuit of the PV module (cell interconnect breaks; corrosion of the junction box, module cables, and connectors); (ii) mechanical damage to the solar cells (cell microcracks and fractures); (iii) PID sustained by the module; and (iv) optical losses affecting the module (soiling, shading, and discoloration).

This was achieved by a set of new diagnostic parameters calculated from the dark I–V characteristic that are sensitive to the degradation of the dark I–V, as well as to shunting and recombination losses. These parameters facilitate the ease of machine analysis for modules degrading nonuniformly across the solar cells, such as modules degrading by PID, or mechanical degradation of the solar cells, and where curve fitting a solar cell model to analyze the degradation mode would not be feasible. These diagnostic parameters, combined with light I–V performance and series-resistance measurements, can enhance the degradation-mode identification possibilities compared to light or dark I–V measurements alone. This enhancement is possible because the new dark I–V diagnostic

parameters show very high sensitivity to shunt and recombination losses while being robust to increased external series-resistance losses, which makes them a great candidate for identifying PID, cell cracks, and cell fractures.

The diagnostic parameters were experimentally validated for each degradation mode discussed, the findings of which were summarized in Table VII. Combining the indicators in Table VII shows a unique signature for every degradation mode that can be used to identify it by combining light I–V with dark I–V measurements.

ACKNOWLEDGEMENTS

The authors thank Garry Babbitt for developing the hardware of the experimental setup; Greg Perrin and Kent Terwilliger for their help performing the experiments; Steve Glick and Steve Rummel for module measurements, as well as Florin Nica, Paul Dan Burlacu, Paula Diaz Reigosa, Stoyan Shivachev, and Viorel Gradea for the partial-shading measurements performed during their student project. This work was realized within the research project "Smart photovoltaic systems", project no. 10648 supported by Energinet.dk, Aalborg University, Otto Mønsteds Fond, as well as the U.S. Department of Energy under Contract No. DE-AC36-08-GO28308 with the National Renewable Energy Laboratory.

REFERENCES

1. EPIA. *Global Market Outlook for Photovoltaics 2014–2018*. European Photovoltaic Industry Association: Brussels, 2013.
2. David F, Galen LB, Robert M, Naïm D, Ted J, Samantha W, Alan G, Ryan HW. Photovoltaic System Pricing Trends: Historical, Recent, and Near-Term Projections - 2013 Edition, 2013.
3. Gilligan C. *The Future Development of the PV Inverter Market*, in *Intersolar Europe Conference*, 2014: Munich, Germany.
4. Meyer EL, van Dyk EE. Assessing the reliability and degradation of photovoltaic module performance parameters. *IEEE Transactions on Reliability* 2004; **53**(1): 83–92. DOI: 10.1109/tr.2004.824831
5. Laukamp H, Schoen T, Ruoss D. Reliability Study of Grid Connected PV Systems, Field Experience and Recommended Design Practice, 2002, International Energy Agency: Freiburg, Germany. p. 31. Report IEA-PVPS T7-08: 2002, iea-pvps.org.
6. Köntges M, Kurtz S, Packard C, Jahn U, Berger KA, Kato K, Friesen T, Liu H, Van Iseghem M. Review of Failures of Photovoltaic Modules, 2014, International Energy Agency. Report IEA-PVPS T13-01:2014, iea-pvps.org.
7. Park NC, Jeong JS, Kang BJ, Kim DH. The effect of encapsulant discoloration and delamination on the electrical characteristics of photovoltaic module. *Microelectronics Reliability* 2013; **53**(9–11): 1818–1822. DOI: 10.1016/j.microrel.2013.07.062
8. Munoz MA, Alonso-García MC, Vela N, Chenlo F. Early degradation of silicon PV modules and guaranty conditions. *Solar Energy* 2011; **85**(9): 2264–2274. DOI: 10.1016/j.solener.2011.06.011
9. Roman E, Alonso R, Ibanez P, Elorduizapatarietxe S, Goitia D. Intelligent PV Module for Grid-Connected PV Systems. *Industrial Electronics, IEEE Transactions on* 2006; **53**(4): 1066–1073. DOI: 10.1109/TIE.2006.878327
10. Sera D, Spataru S, Mathe L, Kerekes T, Teodorescu R. Sensorless PV Array Diagnostic Method for Residential PV Systems. in *26th European Photovoltaic Solar Energy Conference and Exhibition*, 2011. Hamburg, Germany. DOI: 10.4229/26thEUPVSEC2011-4AV.3.37
11. Drews A, de Keizer AC, Beyer HG, Lorenz E, Betcke J, van Sark WGJHM, Heydenreich W, Wiemken E, Stettler S, Toggweiler P, Bofinger S, Schneider M, Heilscher G, Heinemann D. Monitoring and remote failure detection of grid-connected PV systems based on satellite observations. *Solar Energy* 2007; **81**(4): 548–564. DOI: 10.1016/j.solener.2006.06.019
12. Firth SK, Lomas KJ, Rees SJ. A simple model of PV system performance and its use in fault detection. *Solar Energy* 2010; **84**(4): 624–635. DOI: 10.1016/j.solener.2009.08.004
13. Woyte A, Richter M, Moser D, Reich N, Green M, Mau S, Beyer HG. *Analytical Monitoring of Grid-connected Photovoltaic Systems*. International Energy Agency: Brussels, Belgium, 2014. Report IEA-PVPS T13-03: 2014, iea-pvps.org.
14. King DL, Quintana MA, Kratochvil JA, Ellibee DE, Hansen BR. Photovoltaic module performance and durability following long-term field exposure. *Progress in Photovoltaics: Research and Applications* 2000; **8**(2): 241–256. DOI: 10.1002/(SICI)1099-159X(200003/04)8:2<241::AID-PIP290>3.0.CO;2-D
15. Quintana MA, King DL, McMahon TJ, Osterwald CR. Commonly observed degradation in field-aged photovoltaic modules. in *29th IEEE Photovoltaic Specialists Conference*. 2002. New Orleans, USA DOI: 10.1109/PVSC.2002.1190879
16. Kato K. "PVRessQ!" PV Module Failures Observed in the Field, in Photovoltaic Module Reliability Workshop 2012, 2012. National Renewable Energy Laboratory: Golden, Colorado, USA. p. 13–36.
17. Yang BB, Sorensen NR, Burton PD, Taylor JM, Kilgo AC, Robinson DG, Granata JE. Reliability model development for photovoltaic connector lifetime prediction capabilities. in *Photovoltaic Specialists Conference*

(*PVSC*), *2013 IEEE 39th*, 2013. DOI: 10.1109/PVSC.2013.6744115

18. Bowden S, Rohatgi A. Rapid and accurate determination of series resistance and fill factor losses in industrial silicon solar cells. in *17th European Photovoltaic Solar Energy Conference and Exhibition*, 2001. Munich, Germany.
19. Hacke P, Meier DL. Analysis of fill factor losses using current–voltage curves obtained under dark and illuminated conditions. in *29th IEEE Photovoltaic Specialists Conference*, 2002. New Orleans, USA. DOI: 10.1109/Pvsc.2002.1190559
20. Pingel S, Zemen Y, Frank O, Geipel T, Berghold J. Mechanical Stability of Solar Cells within Solar Panels. in *24th European Photovoltaic Solar Energy Conference*, 2009. Hamburg, Germany. DOI: 10.4229/24thEUPVSEC2009-4AV.3.49.
21. Reil F, Althaus J, Vaassen W, Herrmann W, Strohkendl K. The Effect of Transportation Impacts and Dynamic Load Tests on the Mechanical and Electrical Behaviour of Crystalline PV Modules. in *25th European Photovoltaic Solar Energy Conference and Exhibition*, 2010. Valencia, Spain. DOI: 10.4229/25thEUPVSEC2010-4AV.3.9
22. Kajari-Schröder S, Kunze I, Eitner U, Köntges M. Spatial and orientational distribution of cracks in crystalline photovoltaic modules generated by mechanical load tests. *Solar Energy Materials and Solar Cells* 2011; **95**(11): 3054–3059. DOI: 10.1016/j.solmat.2011.06.032
23. Sander M, Dietrich S, Pander M, Schweizer S, Ebert M, Bagdahn J. Investigations on crack development and crack growth in embedded solar cells. in *Reliability of Photovoltaic Cells*, *Modules*, *Components*, *and Systems Conference*, 2011. San Diego, California. DOI: 10.1117/12.893662
24. Buerhop-Lutz C, Schlegel D, Vodermayer C, Nieß M. Quality Control of PV-Modules in the Field Using Infrared-Thermography. in *26th European Photovoltaic Solar Energy Conference and Exhibition*, 2011. Hamburg, Germany. DOI: 10.4229/26thEUPVSEC2011-5AO.5.2
25. Köntges M, Kajari-Schröder S, Kunze I, Jahn U. Crack Statistic of Crystalline Silicon Photovoltaic Modules. in *26th European Photovoltaic Solar Energy Conference and Exhibition*, 2011. Hamburg, Germany. DOI: 10.4229/26thEUPVSEC2011-4EO.3.6
26. Ebner R, Zamini S, Újvári G. Defect Analysis in Different Photovoltaic Modules Using Electroluminescence (EL) and Infrared (IR)-Thermography. in *25th European Photovoltaic Solar Energy Conference and Exhibition*, 2010. Valencia, Spain. DOI: 10.4229/25thEUPVSEC2010-1DV.2.8
27. Pingel S, Frank O, Winkler M, Daryan S, Geipel T, Hoehne H, Berghold J. Potential induced degradation of solar cells and panels. in *35th IEEE Photovoltaic Specialists Conference*, 2010. Honolulu, Hawaii. DOI: 10.1109/PVSC.2010.5616823
28. Berghold J, Koch S, Böttcher A, Ukar A, Leers M, Grunow P. *Potential-induced degradation* (*PID*) *and its correlation with experience in the field*, in *Photovoltaics International*. Solar Media Ltd.: London, 2013; 87–93.
29. Hacke P, Kempe M, Terwilliger K, Glick S, Call N, Johnston S, Kurtz S, Bennett I, Kloos M. Characterization of Multicrystalline Silicon Modules with System Bias Voltage Applied in Damp Heat. in *25th European Photovoltaic Solar Energy Conference and Exhibition*, 2010. Valencia, Spain. DOI: 10.4229/25thEUPVSEC2010-4BO.9.6
30. Schutze M, Junghanel M, Koentopp MB, Cwikla S, Friedrich S, Muller JW, Wawer P. Laboratory study of potential induced degradation of silicon photovoltaic modules. in *Photovoltaic Specialists Conference* (*PVSC*), *2011 37th IEEE*, 2011. DOI: 10.1109/PVSC.2011.6186080
31. Mathiak G, Schweiger M, Herrmann W. Potential-Induced Degradation - Comparison of Different Test Methods and Low Irradiance Performance Measurements. in *27th European Photovoltaic Solar Energy Conference and Exhibition*, 2012. Frankfurt, Germany. DOI: 10.4229/27thEUPVSEC2012-4DO.6.3
32. King DL, Hansen BR, Kratochvil JA, Quintana MA. Dark current–voltage measurements on photovoltaic modules as a diagnostic or manufacturing tool. in *Photovoltaic Specialists Conference*, *1997*, *Conference Record of the Twenty-Sixth IEEE*, 1997. DOI: 10.1109/PVSC.1997.654286
33. Aberle AG, Wenham SR, Green MA. A new method for accurate measurements of the lumped series resistance of solar cells. in *23rd IEEE Photovoltaic Specialists Conference*, 1993. Louisville, Kentucky. DOI: 10.1109/PVSC.1993.347065
34. Köntges M, Kunze I, Kajari-Schröder S, Breitenmoser X, Bjørneklett B. The risk of power loss in crystalline silicon based photovoltaic modules due to micro-cracks. *Solar Energy Materials and Solar Cells* 2011; **95**(4): 1131–1137. DOI: 10.1016/j.solmat.2010.10.034
35. Kajari-Schröder S, Kunze I, Köntges M. Criticality of Cracks in PV Modules. *Energy Procedia* 2012; **27**(0): 658–663. DOI: 10.1016/j.egypro.2012.07.125
36. Breitenstein O, Rakotoniaina JP, Al Rifai MH, Werner M. Shunt types in crystalline silicon solar cells. *Progress in Photovoltaics: Research and Applications* 2004; **12**(7): 529–538. DOI: 10.1002/pip.544
37. van Mölken JI, Yusufoğlu UA, Safiei A, Windgassen H, Khandelwal R, Pletzer TM, Kurz H. Impact of Micro-Cracks on the Degradation of Solar Cell

Performance Based On Two-Diode Model Parameters. *Energy Procedia* 2012; **27**(0): 167–172. DOI: 10.1016/j.egypro.2012.07.046

38. Hacke P, Smith R, Terwilliger K, Glick S, Jordan D, Johnston S, Kempe M, Kurtz S. Testing and Analysis for Lifetime Prediction of Crystalline Silicon PV Modules Undergoing Degradation by System Voltage Stress. *IEEE Journal of Photovoltaics* 2013; **3**(1): 246–253.DOI: 10.1109/Jphotov.2012.2222351
39. Würfel P. *Physics of Solar Cells: From Principles to New Concepts*. Wiley-VCH Verlag GmbH: Weinheim, 2005; 125–127.
40. Lausch D, Naumann V, Breitenstein O, Bauer J, Graff A, Bagdahn J, Hagendorf C. Potential-Induced Degradation (PID): Introduction of a Novel Test Approach and Explanation of Increased Depletion Region Recombination. *Photovoltaics, IEEE Journal of* 2014; **4**(3): 834–840. DOI: 10.1109/JPHOTOV.2014.2300238
41. Werner J. Schottky barrier and pn-junctionI/V plots — Small signal evaluation. *Applied Physics A* 1988; **47**(3): 291–300. DOI: 10.1007/BF00615935
42. Altermatt PP, Heiser G, Aberle AG, Wang A, Zhao J, Robinson SJ, Bowden S, Green MA. Spatially resolved analysis and minimization of resistive losses in high-efficiency Si solar cells. *Progress in Photovoltaics: Research and Applications* 1996; **4**(6): 399–414. DOI: 10.1002/(SICI)1099-159X(199611/12)4:6<399::AID-PIP148>3.0.CO;2–4
43. Hacke P, Terwilliger K, Smith R, Glick S, Pankow J, Kempe M, Bennett SKI, Kloos M. System voltage potential-induced degradation mechanisms in PV modules and methods for test. in *Photovoltaic Specialists Conference* (*PVSC*), *2011 37th IEEE*, 2011. DOI: 10.1109/PVSC.2011.6186079
44. Hacke P, Terwilliger K, Kurtz S. *In-Situ Measurement of Crystalline Silicon Modules Undergoing Potential-Induced Degradation in Damp Heat Stress Testing for Estimation of Low-Light Power Performance*. National Renewable Energy Laboratory (NREL): Golden, CO., 2013. Medium: ED; Size: 10 pp., http://www.osti.gov/scitech//servlets/purl/1090973/, accessed 01/Feb/2014.